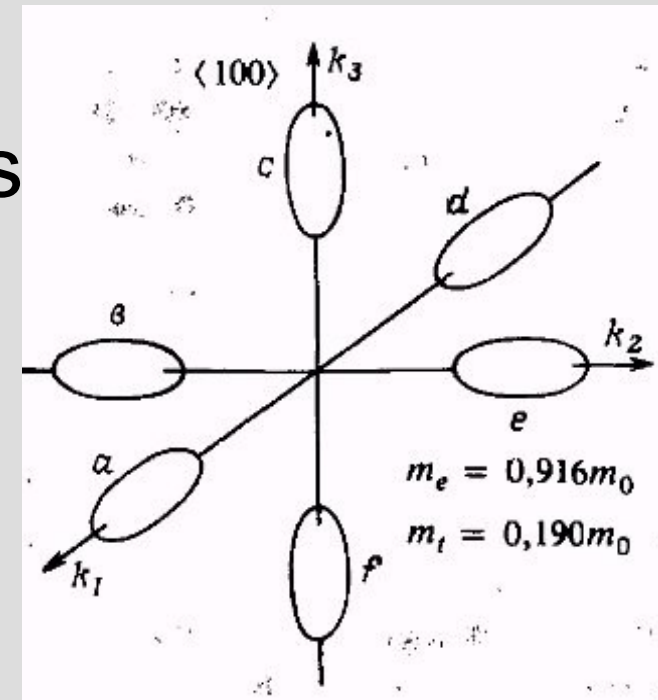
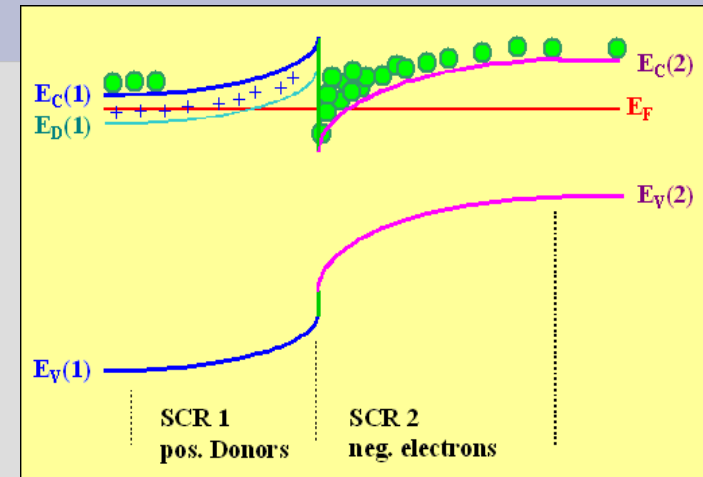


8.513 Lecture 9

**High mobility electron systems:
Different types of 2DEGs
Imaging electron flow
Scattering on a boundary**

Two-dimensional electron systems

- Created on the interfaces in semiconductors by controlled doping or field effect
- Quantum confinement in the perp direction: each discrete level gives a 2D band
- Tunable density of 2D carriers
- Effective mass, g-factor, SO interaction different from 2D bulk
- Valley splitting (e.g. in Si)



Scattering mechanisms

- Coulomb scattering (charge impurities): distant (screened) and local residual impurities (weakly screened)
- Surface roughness Elastic: temperature independent;
Inelastic: decreases at low T
- Intervalley scattering
- Lattice scattering: acoustic phonons, polar optical phonons, phonon-mediated intervalley scattering

Mobility: $j=env$, $v=\mu E$; Drude model: $\mu=(e/m)\tau_{tr}$

in best samples mobility can reach $14000000 \text{ cm}^2/\text{V s}$;

mean free path of up to $120 \mu\text{m}$

3.4 Field effect transistors and quantum wells

The properties of interfaces can be used to construct both useful devices as well as fascinating nanostructures. Field effect transistors are very important in both respects. Many mesoscopic samples are, in one way or another, some sort of field effect transistor, which are frequently denoted by the acronym FET. These devices heavily rely on interface effects. The two most important FETs in our context are the Si-MOSFET and the GaAs-HEMT. These are by no means the only systems though. Particularly in research, a wide variety of heterostructure devices is used. Some examples are given at the end of this section.

3.4.1 The silicon metal-oxide-semiconductor FET (Si-MOSFET)

This type of FET is the basic building block of the vast majority of present-day integrated circuits. A scheme of the Si-MOSFET is shown in Fig. 3.18(a). A silicon chip is, say, p-doped and electrically contacted with two Ohmic contacts that act as source and drain. A metal electrode resides in between the Ohmic contacts, separated by a SiO_2 -layer from the Si. This M-O-S layer sequence can be thought of a Schottky diode of a very high resistance. Currents between the metal electrode and the semiconductor are neglected in the following. With no voltage applied, the resulting band structure across the interface is shown in Fig. 3.18(b). The p-doping is typically rather weak, say $N_D \approx 10^{21} \text{ m}^{-3}$, such that the resistivity of the Si is high. By applying a voltage to the metal electrode with respect to drain, a band bending is induced in the Si, and a corresponding charge accumulation at the $\text{Si} - \text{SiO}_2$ -interface is generated, as depicted for the case of a positive voltage in Fig. 3.18(c). Here, E_c of the Si has dropped below the Fermi level, and electrons collect at the interface in the conduction band. Hence, an electron gas is generated which is confined in z-direction, but free in the directions parallel to the surface. For sufficiently high electron densities in this free electron gas, its conductance is much higher as compared to the p-doped bulk. We speak of *inversion* if the free carrier gas has the opposite sign than the carriers in the bulk due to doping. For appropriate doping densities, we can generate a free hole gas at the O-S interface by applying negative voltages to the metal electrode. This situation is referred to as *accumulation*. Devices which offer the possibility of generating both electron and hole gases are known as *ambipolar*.

The current that flows between source and drain can thus be controlled by the voltage applied to the metal electrode, which is therefore known as the *gate*. The oxide prevents current flow between the gate and the silicon, which would reduce the performance of the switch. This three-terminal device thus represents a transistor that relies on the electrostatic field effect. However, we are not so much interested in the technological applications of MOSFETs in our context. Rather, we focus our attention at the electron gas that has formed at the O-S interface in Fig. 3.18(c). Apparently, its spatial extension in z direction is very small, as we have seen already above. Typically one finds that E_c is below the Fermi level for about 20 nm. Furthermore, the electron densities in such interface layers are much smaller than metallic densities, and the Fermi wavelength is larger. A crude estimation gives $\lambda_F \approx 20 \text{ nm}$. Therefore, we expect size quantization effects in the electron gas. Fig. 3.19 shows a zoom-in of the conduction band structure at the oxide-semiconductor interface. The potential is roughly triangular. By applying an appropriate gate voltage, a situation can be established in which only the energy of the first quantized state is below the Fermi level. Since parallel to

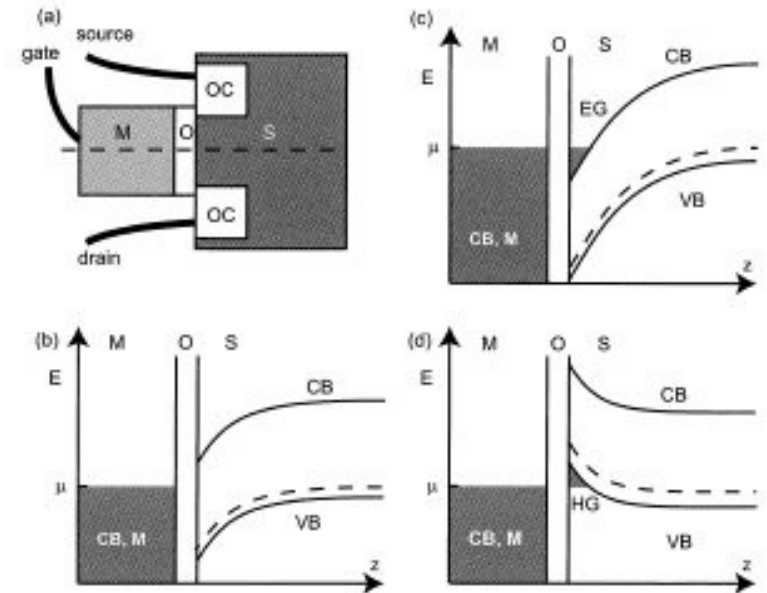


Figure 3.18: (a) Schematic illustration of a silicon MOSFET. A source-drain voltage is applied to a p-doped silicon wafer at two Ohmic contacts (OC). A metal electrode M ("gate") in between the Ohmic contacts is separated from the silicon by a SiO_2 layer. (b) Band alignment across the M-O-S interface (dashed line in (a) for $V_g = 0$). Applying a positive voltage to the gate increases the band bending. Above a threshold gate voltage, the conduction band bottom drops below μ at the O-S interface, and an electron gas (EG) is induced (inversion). A sufficiently large negative gate voltage pulls the top of the valence band above μ , and a hole gas (HG) is generated at the surface (accumulation, (d)).

the interface, the electrons are not confined, a *two-dimensional electron gas* (2DEG) results. The conduction band bottom of this 2DEG is at E_0 in Fig. 3.19. We sometimes speak a two-dimensional subband. If more than one subband is occupied, the electron gas is said to be quasi-two-dimensional.

Like in three dimensions, this electron gas can be described by an effective mass and by the two-dimensional density of states. However, some care is required in adopting the bulk parameters to a two-dimensional carrier gas at an interface. We will meet some of the related issues later on. For now, we just look at the effective electron mass of the 2DEG in the Si-MOSFET. Suppose the Si crystal plane at the interface is a (100) plane, a very common case. The electrons move freely parallel to this plane only. Therefore, it is self-evident to project the valley-degenerated Fermi ellipsoids into that plane, see Fig. 3.20, which results in

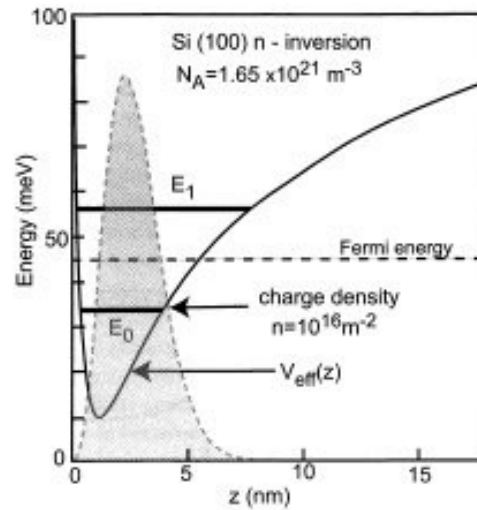


Figure 3.19: Energy diagram of the conduction band in a Si-MOSFET close to the O-S interface, as obtained from a self-consistent calculation that includes electron-electron interactions and screening. In a potential well, quantized states are formed. The resulting electron gas is effectively two-dimensional as long as only the first quantized state lies below the Fermi level. Also indicated is the electronic wave function. After [Ando1976].

4 spin degenerate ellipses and a twofold valley-degenerated and spin degenerate circle at the center. Due to interface effects, however, the degeneracy between the ellipses and the circles gets removed, and the conduction band at the circle is about 20 meV below the conduction band minimum in the ellipses [Ando1982]. At room temperatures, both types of minima are occupied. At low temperatures, however, i.e. for $\Theta < 4.2$ K the electrons have a single effective mass of $m^* = 0.19m_e$ parallel to the surface, and the valley degeneracy is reduced to 2.

The two-dimensionality of this interface electron gas has some most surprising consequences, as will be seen in Chapter 6. But this is not the sole interesting property of such electron gases. Furthermore, the electron densities are much smaller than in conventional metals, and can be tuned. The Fermi wavelength is comparatively large, and size quantization effects can be expected also laterally, provided the MOSFET is patterned accordingly. Also, low density means that electron-electron interactions are more important, due to reduced screening.

Since the electrons are to some degree spatially separated from the ionized donors, impurity scattering is reduced and the electron mobility increases. In fact, the mobility of an electron gas at a O-S interface can be two orders of magnitude larger than the mobility of bulk Si. The mobility is typically dominated by scattering at impurities embedded in the ox-

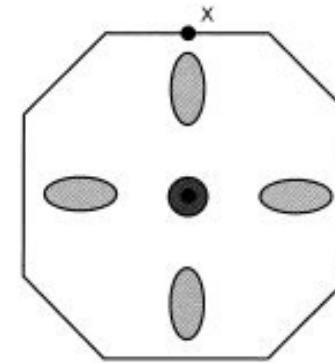


Figure 3.20: Projection of the Si Fermi surface for typical electron densities onto a (100) plane. Two ellipsoids get projected onto the Γ point. Their energy is reduced as compared to the 4 projected ellipses due to interface effects.

ide. Furthermore, the oxide is amorphous. The oxide atoms are by no means periodically arranged, which will cause additional electron scattering. However, due to size quantization, the probability of finding electrons right at the O-S interface is reduced, see the wave function in Fig. 3.19. The maximum of the probability density is several nanometers away from the interface.

3.4.2 The Ga[Al]As high electron mobility transistor (GaAs-HEMT)

In this system, the two-dimensional electron gas is generated inside the GaAs, at the interface formed between $\text{Al}_x\text{Ga}_{1-x}\text{As}$ and GaAs. The band alignment of this interface is of type I. The band offsets depend on x , see Fig. 2.6. A typical choice is $x=0.3$. In that case, the conduction band of $\text{Al}_{0.3}\text{Ga}_{0.7}\text{As}$ is 300 meV above that one of GaAs. The top of the $\text{Al}_{0.3}\text{Ga}_{0.7}\text{As}$ valence band is located about 160 meV below that one of GaAs. This is of no further interest here, as we are going to consider again an electron gas.

In contrast to Si, the GaAs remains undoped. Instead, the electrons are provided by a doping layer inside the $\text{Al}_{0.3}\text{Ga}_{0.7}\text{As}$. Usually, Si is used as a donor. The doping layer can be spatially separated from the $\text{Al}_{0.3}\text{Ga}_{0.7}\text{As}$ by several tens of nanometers, see Fig. 3.21 (a). While most of the doping electrons that get thermally excited into the conduction band occupy the nearby surface states, some of them (typically about 10 %) reduce their energy by falling across the interface into the GaAs conduction band. This doping technique is called modulation doping; it was first demonstrated by [Dingle1978]. An accurate doping density is essential in designing a good HEMT structure: only a few percent deviation from the correct doping density can either cause mobile electrons in the doping layer (a "bypass"), or the triangular potential at the heterointerface remains empty. While the doping density and the thickness of the spacer layer determine the density of the 2DEG, it can be tuned with a top

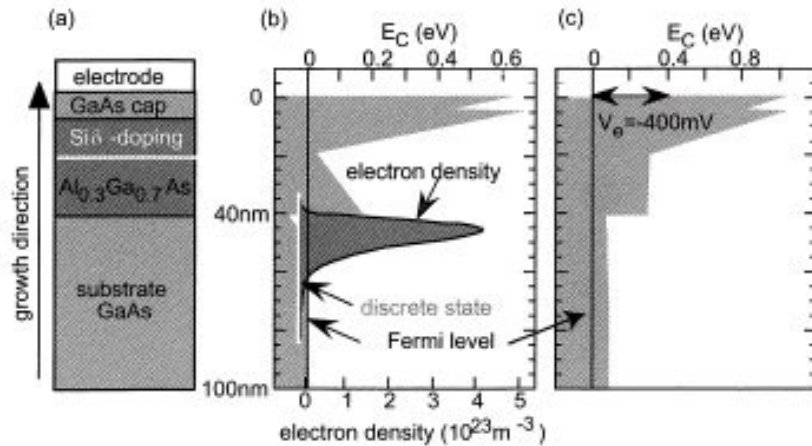


Figure 3.21: (a): band alignment at a modulation doped $GaAs - Al_xGa_{1-x}As$ interface. (b): schematic structure of a GaAs HEMT with the gate electrode grounded. (c) For gate voltages below $-400mV$, E_C at the interface moves above the chemical potential, and the electron gas is depleted.

gate over wide ranges.

Consequently, two charge dipoles build up, one between the surface and the doping layer, and a second one between the GaAs - $Al_{0.3}Ga_{0.7}As$ heterointerface.⁷ This results in the band structure sketched in 3.21 (b). As in the Si-MOSFET, the resulting electron gas can be two-dimensional, and its carrier density can be tuned by applying voltages to a gate on top of the heterostructure, see Fig. 3.21 (c). Thus, the electron gas is present in this structure if no gate voltage is applied, or if there is no gate at all. Modulation doping of GaAs heterostructures caused a big progress in the electron mobilities that could be achieved (Fig. 3.22). The reason is twofold. First of all, $Al_xGa_{1-x}As$ is quasi-crystalline, in contrast to the SiO_2 - layer in a Si-MOSFET. Although the Al atoms replace the Ga atoms at random sites, this ternary compound is a somewhat distorted zincblend crystal structure with a well-defined lattice constant. The lattice mismatch between GaAs and $Al_{0.3}Ga_{0.7}As$ is only 0.4 %. Hence, the electrons in the 2DEG see an almost perfectly periodic environment, and the interface causes much less scattering as compared to the O - S interface in a Si-MOSFET. Second, the ionized donors, which are a strong source of scattering, are spatially separated from the electron gas. Consequently, the screened Coulomb potentials the electrons see are much weaker and generate predominantly small-angle scattering. In the years 1978 to 1985, the layer sequences and the compositions of Ga[Al]As-HEMTs had been optimized, and the increase in low-temperature electron mobilities achieved in this period is truly remarkable, see Fig.3.22. Today, the world

⁷Note the thin GaAs cap layer at the surface. Its purpose is to avoid oxidation of the $Al_{0.3}Ga_{0.7}As$ layer when exposed to air.

record is $\mu = 1440m^2/Vs$, held by [Umansky1997]. This corresponds to a mean free path of $120 \mu m$. Although very similar devices can be built of several materials, like, e.g. Ga[Al]N, the Ga[Al]As heterostructure has remained unsurpassed in terms of electron mobility.

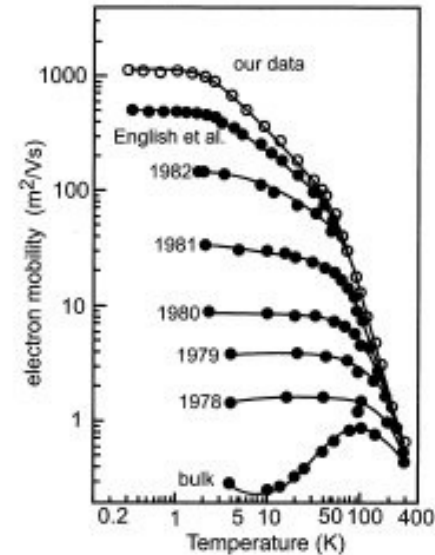


Figure 3.22: Evolution of electron mobilities over time, after modulation doping was introduced. After [Pfeiffer1989].

Another advantage of the Ga[Al]As system is the possibility to design the spatial variation of the band structure by controlling the Al content during sample growth. For example, quantum wells can be grown by embedding a thin layer of GaAs in two $Al_{0.3}Ga_{0.7}As$ layers. Varying the Al content parabolically during growth, i.e. $x \propto (z - z_0)^2$, results in a parabolic quantum well in growth direction, see 3.23. Hence, quantum mechanical model potentials can be experimentally realized this way, as long as the envelope function approximation is reasonable. We will occasionally meet such structures later on.

3.4.3 Other types of layered devices

We conclude this section with a selection of further interesting heterostructures. In particular, the Si[Ge] quantum well and the InAs/AlSb quantum wells are presented. Also, we will have a look at organic FETs. The materials cannot be combined arbitrarily, though. The lattice constants of the two components that form the interface should differ as little as possible. Differences in the lattice constants will inevitably lead to strained layers, which generates lattice dislocations and thus additional scattering. If the strain gets larger than $\approx 1\%$ homogeneous film growth is no longer possible, and strained islands of one material form instead. While

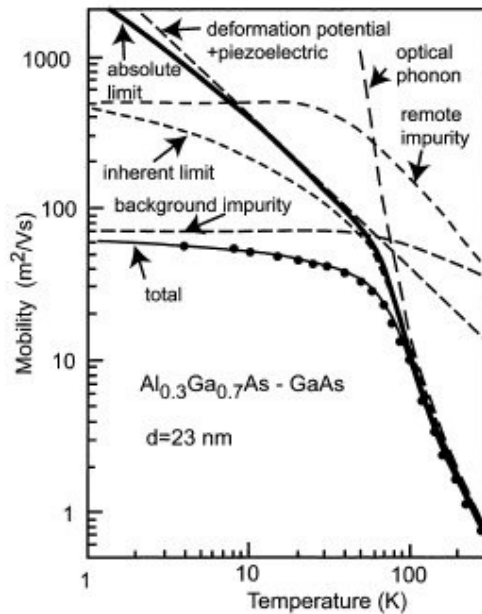


Figure 3.28: Significance of various scattering processes in a Ga[Al]As-HEMT. Black dots denote experimental results for a typical structure, with an electron density of $n = 2.2 \times 10^{15} \text{ m}^{-2}$, and a spacer thickness of $d=23 \text{ nm}$. The density of the modulation doping was $8.6 \times 10^{22} \text{ m}^{-3}$. This doping, which causes the remote impurities, was present within a 20 nm - layer between the surface and the spacer. In addition, a homogeneous density of background impurities of $9 \times 10^{19} \text{ m}^{-3}$ was assumed, which is a typical number for high-quality GaAs. After [Walukiewicz1984].

in the limit of low temperatures (see eq. (2.51) for the three-dimensional case) is given by

$$\epsilon(\vec{q}) = \begin{cases} 1 + \frac{k_{TF}}{q} & q \leq 2k_F \\ 1 + \frac{k_{TF}}{q} \sqrt{1 - \left(\frac{2k_F}{q}\right)^2} & q > 2k_F \end{cases} \quad (3.23)$$

and the resulting charge density induced by a Coulomb potential reads at large distances from the scattering center

$$V_{eff}(\vec{r}) = \frac{Ze}{\epsilon\epsilon_0} \frac{4k_{TF}k_F^2}{(2k_F + k_{TF})^2} \frac{\sin(2k_F r)}{(2k_F r)^2} \quad (3.24)$$

Thus, the screened potential drops with r^{-2} as compared to r^{-3} in three dimensions.

Furthermore, additional scattering mechanisms, which are absent in bulk materials, are possible in quantum confined systems. The scattering of electrons on ionized impurities has

a somewhat different character in modulation doped systems as compared to bulk materials, since they are spatially separated from the electrons by a spacer layer. The residual and usually small density of ionized impurities inside the electron gas is comparatively small in high quality systems. One may be tempted to guess that the broader the spacer layer, the higher the mobility. This is not the case, though, since as the spacer thickness becomes larger, the carrier density gets smaller, and screening becomes less effective. Hence, a maximum in the mobility as a function of the spacer thickness is observed. In Ga[Al]As-HEMTs, the optimum spacer thickness depends on the cleanliness of the material and the doping density. It varies between $\approx 20 \text{ nm}$ and $\approx 60 \text{ nm}$. Another scattering mechanism in FET structures is interface roughness scattering. The interface clearly constitutes a deviation from perfect periodicity and consequently generates scattering. In case of a Ga[Al]As HEMT, this is of minor importance. In narrow quantum wells, however, where fluctuations at both interfaces are important, this mechanism may become important. In Si-MOSFETs, on the other hand, the oxide is amorphous, and interface roughness scattering is not negligible.

Alloy scattering occurs in compound materials such as $\text{Al}_x\text{Ga}_{1-x}\text{As}$. The replacement of Ga atoms by Al atoms takes place at random positions, and a non-periodic potential results. This kind of scattering usually plays no significant role, as long as the carriers reside in a crystalline material, such as GaAs, with a barrier made of a ternary compound, since only the evanescent tails of the wave function feel this kind of disorder. In Fig. 3.28 a model

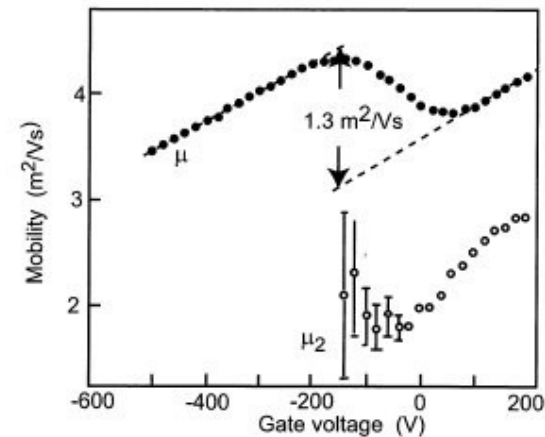
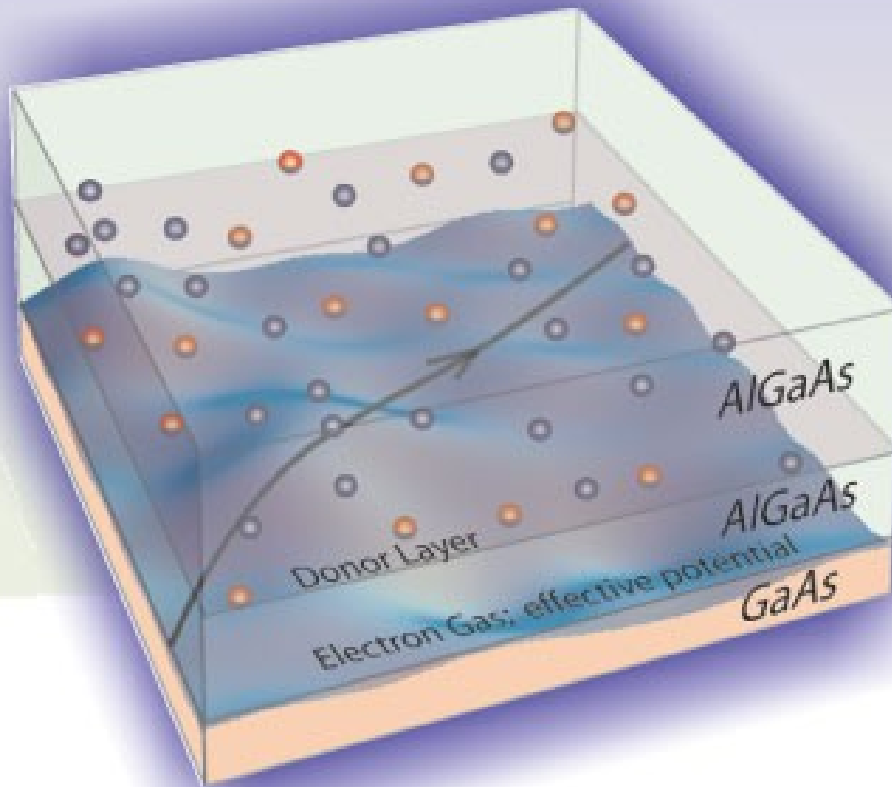


Figure 3.29: Electron mobilities in a GaAs-HEMT as a function of the gate voltage. Above a threshold electron density, the second two-dimensional subband gets occupied, and the mobility drops due to additional intersubband scattering. After [Stormer1982].

calculation adopted to some typical data is shown, which surveys the relevance of various scattering mechanisms in a Ga[Al]As-HEMT. While alloy scattering and interface roughness scattering are irrelevant except at very low temperatures and in extremely clean samples, the ionized impurities are split into two components, namely a density of homogeneously dis-

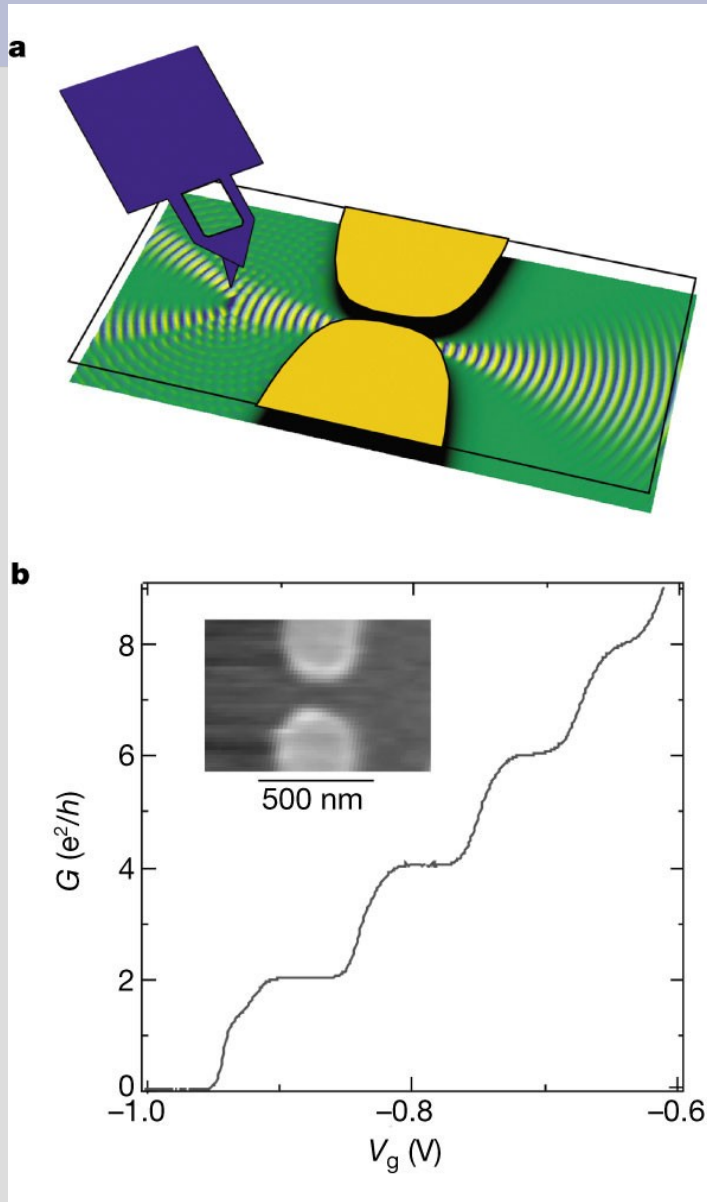
Imaging electron flow through a QPC in a high mobility 2DEG

Disorder potential and electron trajectory in a 2DEG: mostly small-angle scattering



A two-dimensional electron gas formed at the interface between gallium arsenide and aluminum gallium arsenide in a semiconductor heterostructure. The AlGaAs layer (green) contains a layer (purple) of silicon donor atoms (dark blue). Electrons from the donor layer fall into the GaAs layer (pink) to form a 2DEG (blue) at the interface. The ionized Si donors (red) create a potential landscape for the electron gas; the resulting small-angle scattering smoothly bends electron trajectories, as shown. (from: Topinka, Westervelt, Heller, *Physics Today* December 2003)

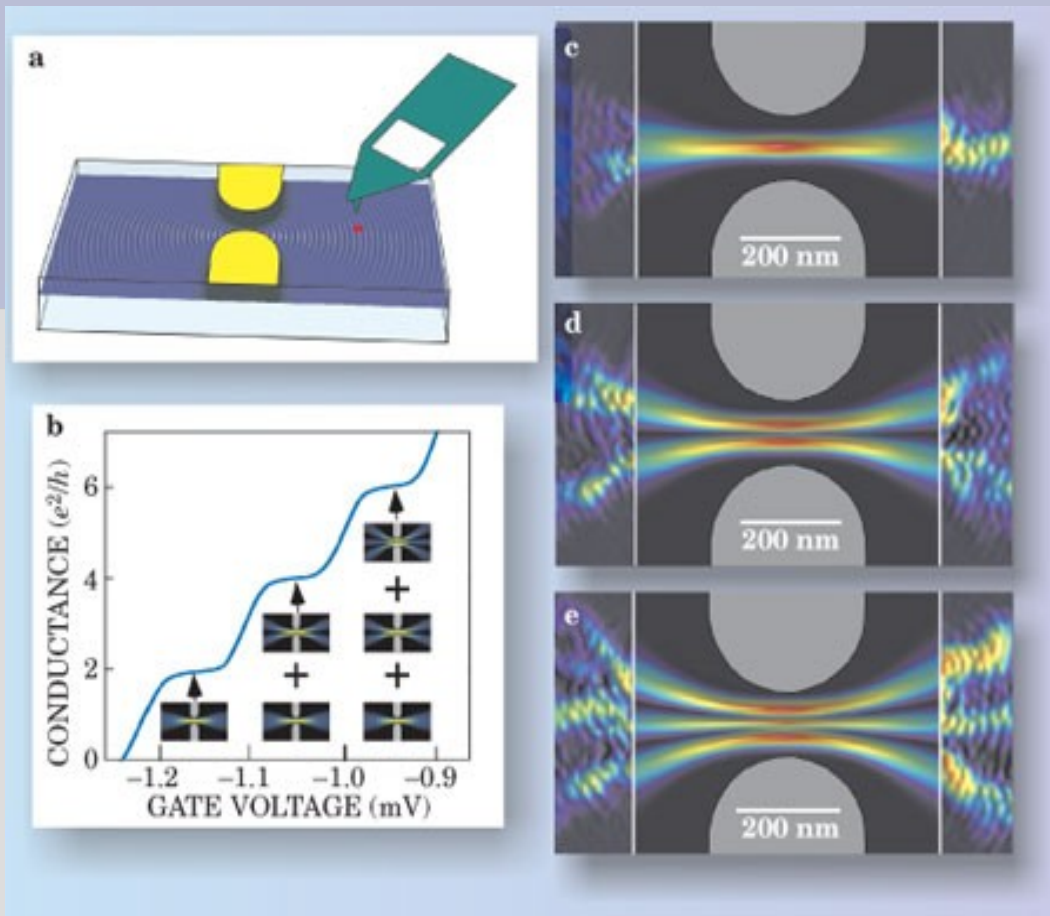
Response to a remote local probe



Topinka et al, Nature 410, 183 (2001)

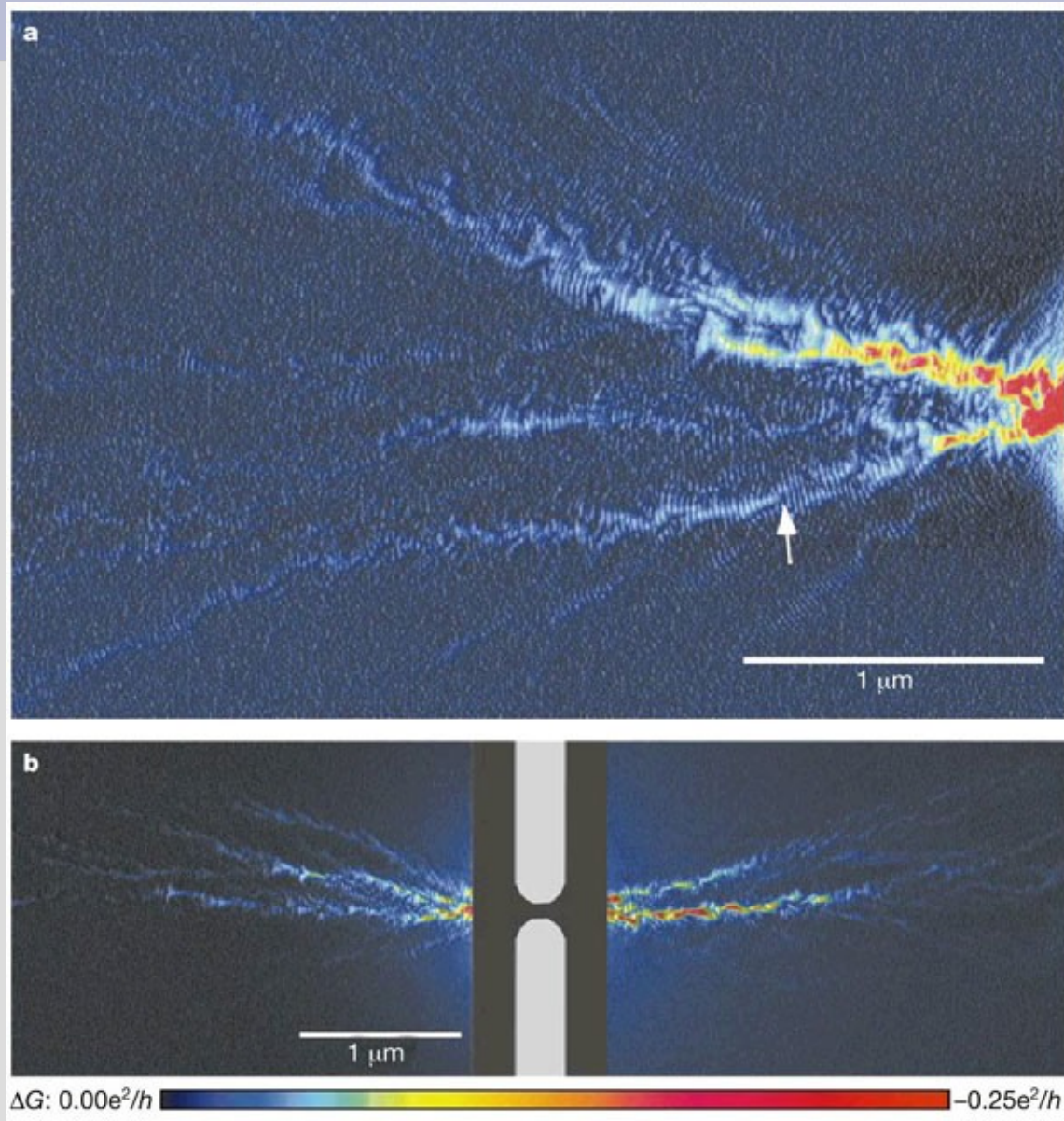
a, Schematic diagram of the experimental set-up used for imaging electron flow. **The tip introduces a movable depletion region which scatters electron waves flowing from the quantum point contact (QPC).** An image of electron flow is obtained by measuring the effect the tip has on QPC conductance as a function of tip position. Two ohmic contacts approx 1 mm away from the QPC (not shown) allow the conductance of the QPC to be measured using an a.c. lock-in amplifier at 11 kHz. The root-mean-square voltage across the QPC, 0.2 mV, was chosen in order not to heat electrons significantly above the lattice temperature of 1.7 K.

b, Conductance of the QPC used for Fig. 2b versus QPC width controlled by the gate voltage. Steps at integer multiples of $2e^2/h$ are clearly visible. The inset is a topographic AFM image of the QPC.



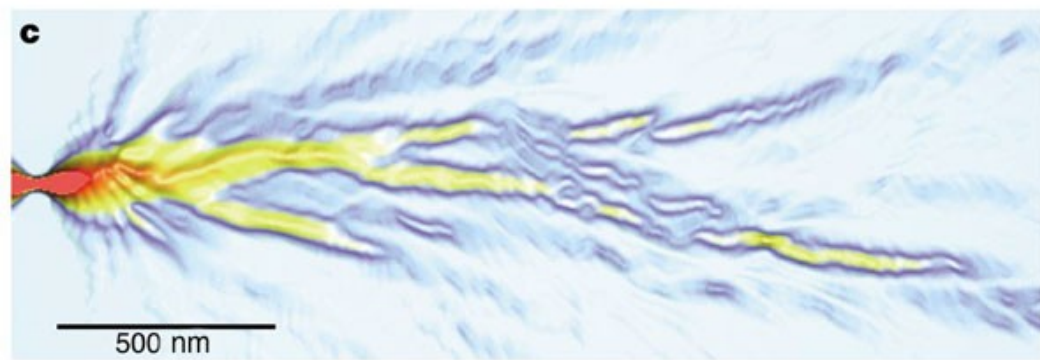
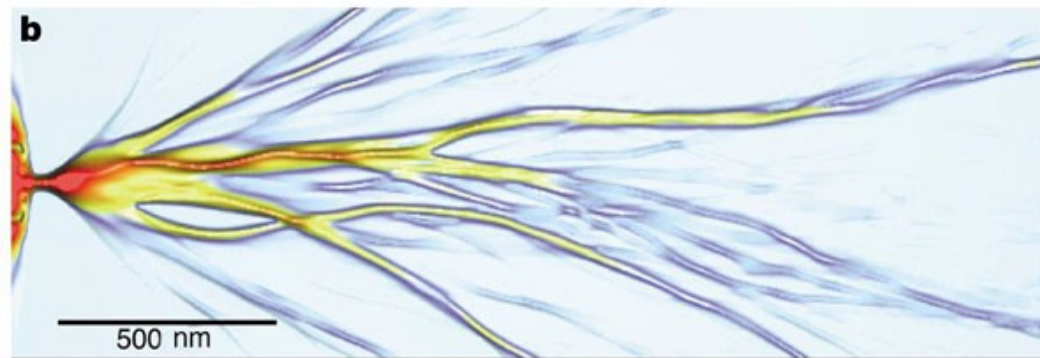
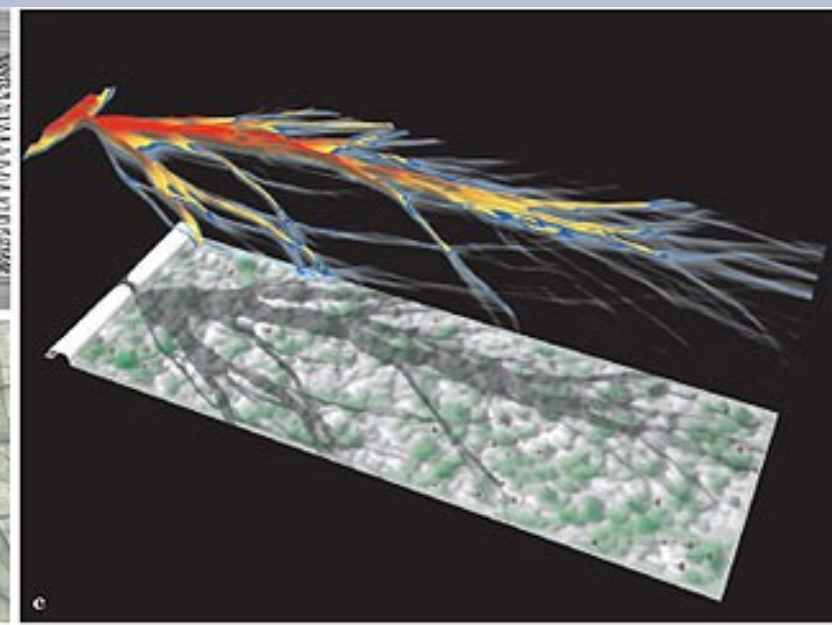
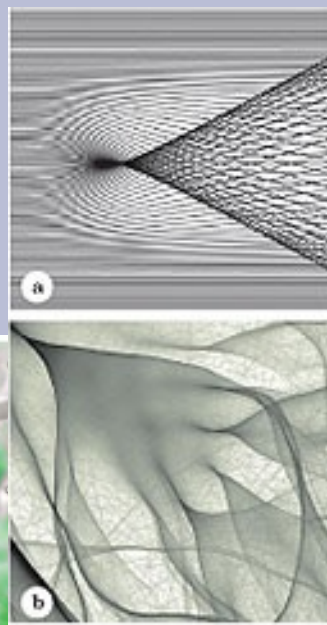
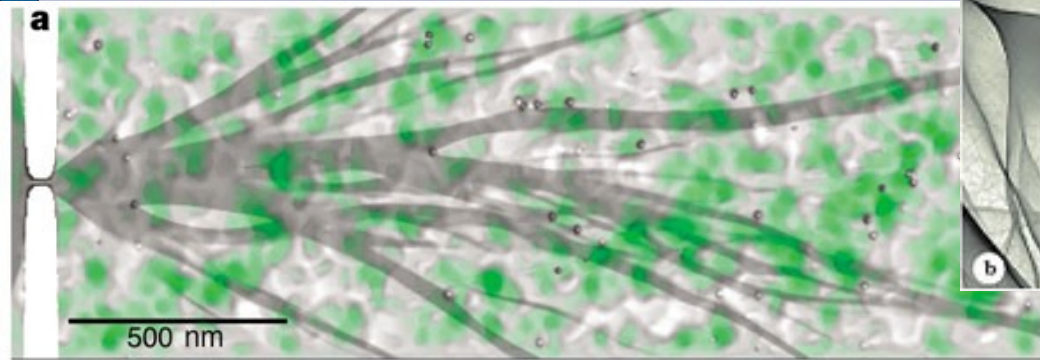
Electron flow through a quantum point contact. (a) Scheme for imaging current flow through a QPC using scanning probe microscopy. Two gate electrodes (yellow) create a narrow constriction in the underlying two-dimensional electron gas. A charged tip (green) depletes the electron gas below it, creating a divot (red spot) that scatters incoming electron waves, as shown in the simulations (blue). (b) The conductance of the QPC, measured at 1.7 K, increases in quantized steps as the gate voltage (and QPC width) is increased. The insets below each step show simulations of the spatial pattern of electron flow for the transverse modes that contribute to the conductance. (c-e) Experimental images of electron flow at 1.7 K (left and right) and theoretical simulations (center) for the first three transverse modes of a QPC. The observed interference fringes spaced by half the Fermi wavelength demonstrate the coherence of electron flow. Because the additional flow, appearing as the QPC becomes wider, is due to the newly opened-up mode, the image for each transverse mode could be obtained by subtracting the raw images from the next lower step.

Experimental images of electron flow. Image of electron flow from one side of a QPC at $T = 1.7$ K, biased on the $G = 2e^2/h$ conductance step.



Dark regions correspond to areas where the tip had little effect on QPC conductance, and hence are areas of low electron flow. The colour varies and the height in the scan increases with increasing electron flow. Narrow branching channels of electron flow are visible, and fringes spaced by $\lambda F/2$, half the Fermi wavelength, are seen to persist across the entire scan. b, Images of electron flow from both sides of a different QPC, again biased on the $G = 2e^2/h$ conductance step. The gated region in the centre was not scanned. Strong channelling and branching are again clearly visible. The white arrow points out one example of the formation of a cusp downstream from a dip in the potential.

Calculated electron flow: branching strands, V-shaped cusps, focusing by ripples.



Surface plot of the random potential for computed electron flow, including contributions from impurities, donors, and gates; green areas are low and white areas are high potential. The 'shadow' is cast by classical flux through the same potential. We note that the branched flux does not follow valleys in the potential. b, Classical and c, quantum-mechanical flux of electrons flowing through the potential in a. In the classical case, we followed the dynamics of an appropriate ensemble of classical trajectories and show the classical flux density. The quantum-mechanical results show the flux density of the transmitted wavefunction, coming through the point contact on the left. We note that both results show the same branching behaviour.

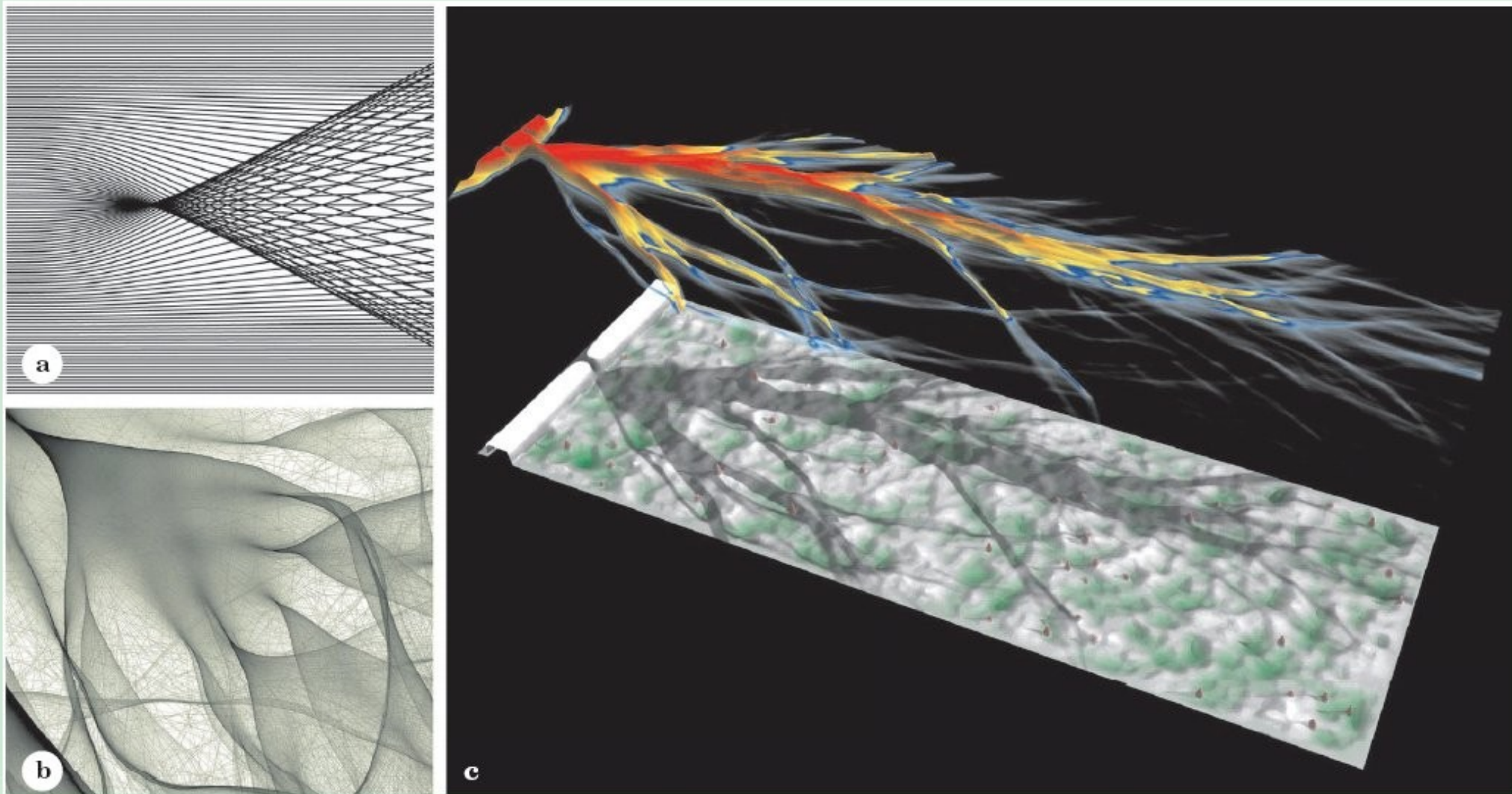


Figure 6. Simulations of electron flow. (a) Parallel electron trajectories, going from left to right, form a V-shaped cusp due to focusing by a potential-energy dip caused by a charged donor atom (not seen) above a two-dimensional electron gas. (b) A realistic 2DEG simulation that includes many ionized donors forms several generations of cusps. The electrons travel here from upper left to lower right. (c) Ray-tracing simulations of electron flux emerging from a small opening into a region of random potential reflect the features seen in experimental images of 2DEG quantum point contact samples. The potential is shown green in the valleys and white on the peaks. The electron flux is coded by height and color, with blue corresponding to regions of low flux; still lower flux is transparent. The “shadow” of the flux on the potential plot shows where the flux lies relative to the hills and valleys; no guiding valleys are seen. A slight change of the position of the opening changes the location and direction of the branches. (S. E. J. Shaw, PhD thesis, Harvard University, 2002.)

QM model reproduces fringes spaced by $\lambda_F/2$

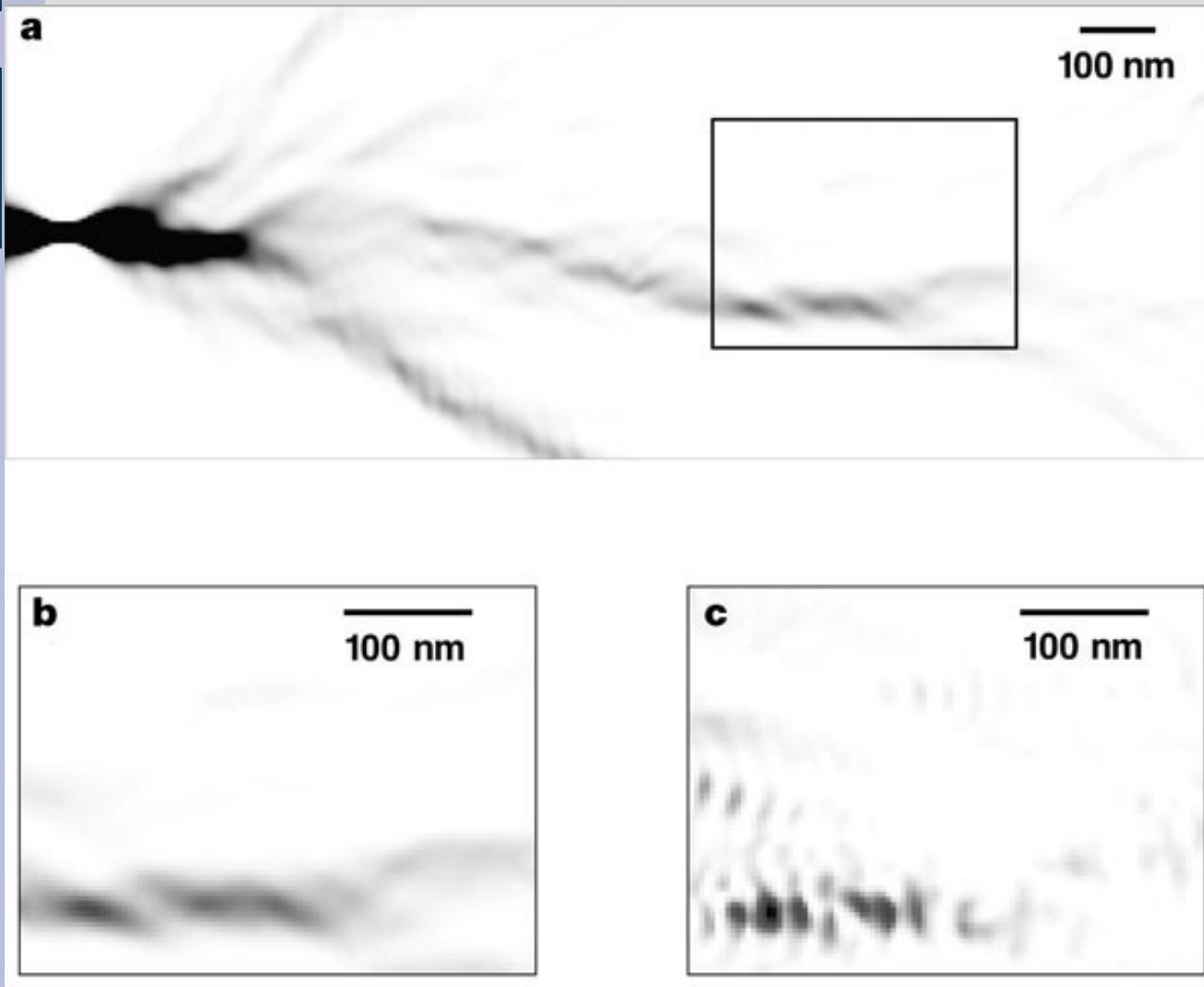


Figure 4: Calculated tip scan. a, Quantum-mechanical flux through a random potential. b, The flux from the boxed area in a. c, A raster scan of conductance as a function of SPM tip position in the same system as a and b. The conductance image in the model corresponds to the flux image, confirming our assertion that the experiment images electron flow. Additionally, the simulation c shows quantum fringes, as seen in the experiment. Though this simulation is at zero temperature, the fringes do survive thermal averaging.

Features

- Angular dependence of the flow agrees with the structure of quantized modes in a QPC
- Observe branched flow with V-shape cusps
- Consistent with earlier results on transport indicating dominant small-angle scattering
- Quantum coherence: fringes spaced by half-a-wavelength

?

Boundary scattering

- Specular scattering (parallel momentum conserved): resistance unaffected, retains the bulk Drude value;
- Diffuse scattering (velocity fully randomized at each scattering on the boundary): resistance increased;
- In a narrow channel the channel width is effectively a mean free path for boundary scattering;
- A more general (heuristic) model: each electron reflected specularly with probability p and diffusely with probability $1-p$

Boltzmann equation

In a channel with hard walls at $x=+W/2, -W/2$ and diffuse scattering, write stationary Boltzmann eqn

$$\mathbf{v} \cdot \frac{\partial}{\partial \mathbf{r}} F = -\frac{1}{\tau} F + \frac{1}{\tau} \int_0^{2\pi} \frac{d\alpha}{2\pi} F,$$

$$\mathbf{r} \equiv (x, y) \quad \mathbf{v} \equiv v_F (\cos \alpha, \sin \alpha)$$

The boundary condition at $x=+W/2, -W/2$:

Find solution corresponding to constant density gradient along the channel:

$$F(\mathbf{r}, \alpha) = \frac{1}{2} \int_{-\pi/2}^{\pi/2} d\alpha' F(\mathbf{r}, \alpha') \cos \alpha',$$

for $x = \frac{W}{2}, \frac{\pi}{2} < \alpha < \frac{3\pi}{2},$

$$= \frac{1}{2} \int_{\pi/2}^{3\pi/2} d\alpha' F(\mathbf{r}, \alpha') \cos \alpha',$$

for $x = -\frac{W}{2}, -\frac{\pi}{2} < \alpha < \frac{\pi}{2}.$

$$F(\mathbf{r}, \alpha) = -cy + cl \sin \alpha \left[1 - \exp \left(-\frac{W}{2l |\cos \alpha|} - \frac{x}{l \cos \alpha} \right) \right],$$

$$l \equiv v_F \tau.$$

The diffusion current

$$I_y = v_F \int_{-W/2}^{W/2} dx \int_0^{2\pi} d\alpha F \sin \alpha$$

Classical size effect in resistivity

General expression for resistivity in terms of the bulk value ρ_0 :

$$\rho = \rho_0 \left[1 - \frac{4l}{\pi W} \int_0^1 d\xi \xi (1 - \xi^2)^{1/2} (1 - e^{-W/l\xi}) \right]^{-1}$$

A log-divergence!
Electrons propagating nearly parallel to the channel travel over large distances without collisions and effectively shortcircuit current

For $l/W \ll 1$ one has

$$\rho = \rho_0 \left(1 + \frac{4}{3\pi} \frac{l}{W} \right),$$

For $l/W \gg 1$ one has asymptotically

$$\rho = \frac{\pi}{2} \rho_0 \frac{l}{W} \frac{1}{\ln(l/W)} = \frac{\pi}{2} \frac{mv_F}{n_s e^2 W} \frac{1}{\ln(l/W)}$$

The effect of magnetic field

- Trajectories bend in weak fields, enhancing scattering (“ballistic” carriers eliminated)
- In strong fields, backscattering suppressed, forward/backward trajectories at $x=+W/2, -W/2$

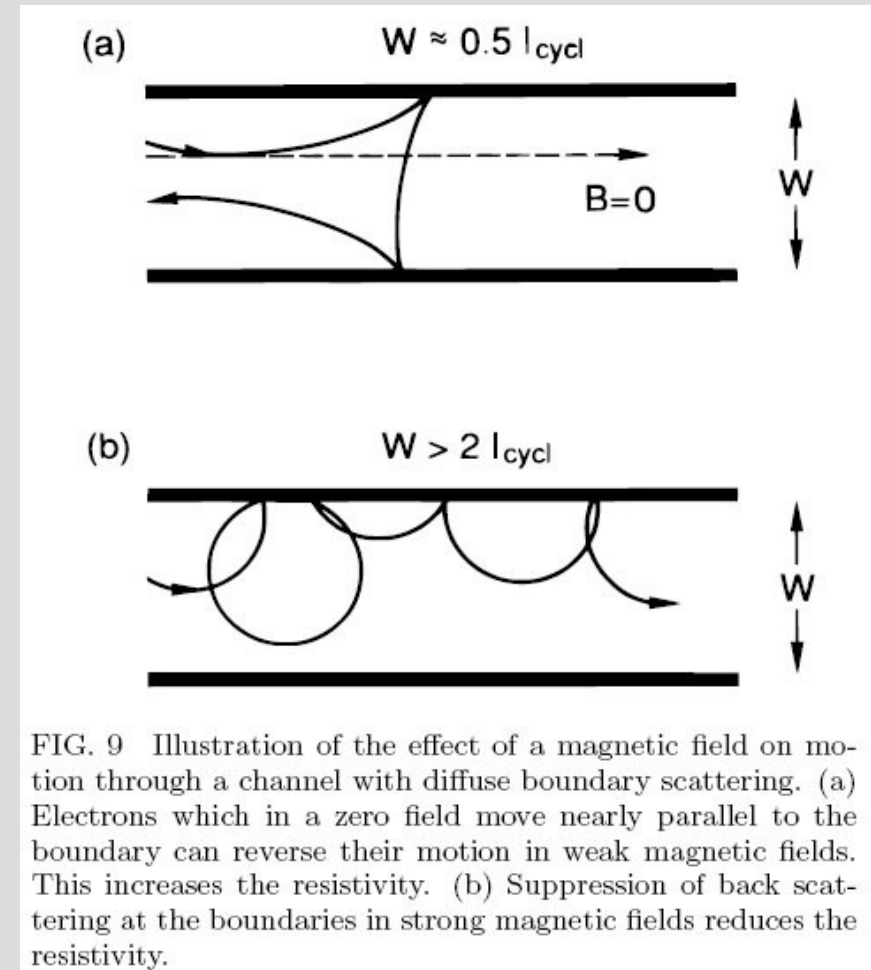


FIG. 9 Illustration of the effect of a magnetic field on motion through a channel with diffuse boundary scattering. (a) Electrons which in a zero field move nearly parallel to the boundary can reverse their motion in weak magnetic fields. This increases the resistivity. (b) Suppression of back scattering at the boundaries in strong magnetic fields reduces the resistivity.

Magnetoresistance positive at low B, negative at high B

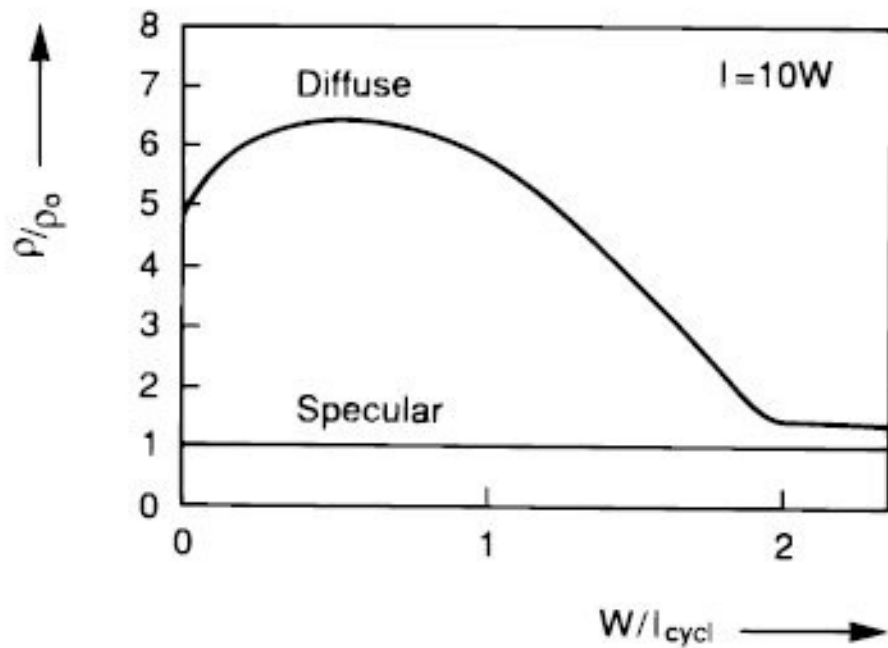


FIG. 10 Magnetic field dependence of the longitudinal resistivity of a channel for the two cases of diffuse and specular boundary scattering, obtained from the Boltzmann equation in the scattering time approximation.

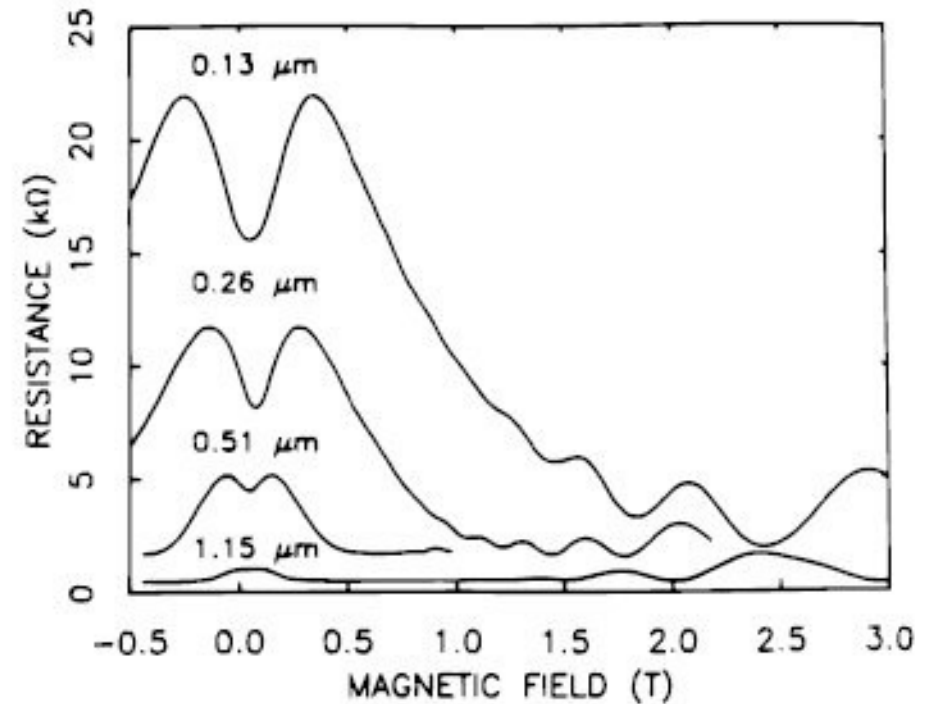


FIG. 11 Experimental magnetic field dependence of the resistance of channels of different widths, defined by ion beam exposure in the 2DEG of a GaAs-AlGaAs heterostructure ($L = 12 \mu\text{m}$, $T = 4.2 \text{K}$). The nonmonotonic magnetic field dependence below 1 T is a classical size effect due to diffuse boundary scattering, as illustrated in Fig. 9. The magnetoresistance oscillations at higher fields result from the quantum mechanical Shubnikov-De Haas effect. Taken from T. J. Thornton et al., Phys. Rev. Lett. **63**, 2128 (1989).